



## Article

# Influence of Ultrasound on the Properties of Polysaccharide Complexes and Materials Based on Them

Elizaveta Mokhova <sup>1</sup>, Mariia Gordienko <sup>1,\*</sup>, Natalia Menshutina <sup>1</sup>, Sergei Kalenov <sup>2</sup>, Igor Avetissov <sup>3</sup> and Artyom Ereemeev <sup>4</sup>

<sup>1</sup> The Department of Chemical and Pharmaceutical Engineering, Mendeleev University of Chemical Technology of Russia (MUCTR), 125047 Moscow, Russia; mokhova.e.k@muctr.ru (E.M.); menshutina.n.v@muctr.ru (N.M.)

<sup>2</sup> The Department of Biotechnology, Mendeleev University of Chemical Technology of Russia (MUCTR), 125047 Moscow, Russia; kalenov.s.v@muctr.ru

<sup>3</sup> The Department of Chemistry and Technology of Crystals, Mendeleev University of Chemical Technology of Russia (MUCTR), 125047 Moscow, Russia; avetisov.i.k@muctr.ru

<sup>4</sup> Federal Scientific and Clinical Center, Malaya Pirogovskaya, 119435 Moscow, Russia; art-eremeev@yandex.ru

\* Correspondence: gordienko.m.g@muctr.ru; Tel.: +7-495-495-0029

**Abstract:** Freeze-drying is often used as a final stage to produce three-dimensional porous matrices for medicine. Because a pure solvent crystallizes first during freezing, it acts as a pore-forming agent. The size of the solvent crystals primarily depends on the cooling rate and the composition of the material to be frozen. Ultrasonic treatment also affects the size of crystals and can be used to control the structure of a porous matrix. This article describes the effect of ultrasound (40 kHz, 50 W) applied at the preliminary freezing stage of polysaccharide solutions (alginate, chitosan, alginate–chitosan and alginate–gelatin) on the finished matrix properties. The most attention was paid to the effect of ultrasound on the size and shape of crystals formed during freezing, which leads to a change in the porous structure of the matrices after solvent sublimation. As a result of changes in the microstructure, a number of differences in the vibrational spectra of the molecules and the values of pore volume, sorption capacity, permeability and degradation of matrices were identified. Such changes in the structure of materials, as well as the emerging directionality of pores, together can affect the process of cell cultivation in these polysaccharide matrices, which can be useful in solving problems of tissue engineering.

**Keywords:** polysaccharides; sodium alginate; chitosan; matrices; ultrasonic treatment; a set of properties; change in microstructure; cell cultivation



**Citation:** Mokhova, E.; Gordienko, M.; Menshutina, N.; Kalenov, S.; Avetissov, I.; Ereemeev, A. Influence of Ultrasound on the Properties of Polysaccharide Complexes and Materials Based on Them. *Polysaccharides* **2023**, *4*, 189–208. <https://doi.org/10.3390/polysaccharides4030014>

Academic Editor: Ylenia Zambito

Received: 30 May 2023

Revised: 24 June 2023

Accepted: 28 June 2023

Published: 30 June 2023



**Copyright:** © 2023 by the authors. Licensee MDPI, Basel, Switzerland. This article is an open access article distributed under the terms and conditions of the Creative Commons Attribution (CC BY) license (<https://creativecommons.org/licenses/by/4.0/>).

## 1. Introduction

The development of materials based on natural polymers is a rather promising task for medicine, pharmaceuticals, biotechnology, and tissue engineering [1,2]. Polysaccharides and polymers of protein origin are widely used in this area [3–6]: sodium alginate, chitosan, pectin, gelatin, collagen and many others. These polymers are used in the production of medical matrices and various types of composite materials for cell culture and regenerative medicine, as well as in the creation of drug delivery systems [3,7–12].

The combination of different properties of polymers contributes to the development of new hybrid and composite materials. For example, sodium alginate, which has a high sorption capacity, is able to form polyelectrolyte complexes with chitosan, which, in turn, has bactericidal properties associated with the presence of a large number of free amino groups in the chitosan molecule [9]. The ability of chitosan to form a large number of hydrogen bonds makes it possible to bind water-soluble organic substances, including bacterial toxins [9,13]. The combination of the properties of sodium alginate and chitosan

in one material made it possible to develop hemostatic agents [14] in the form of sponges, as well as scaffolds for neural tissue engineering [15]. In turn, the combination of the properties of collagen and chitosan, as well as gelatin and chitosan, contributed to the development of scaffolds for skin regeneration and matrices for cell cultivation *in vitro*, respectively [10,16–18]. When developing new materials, combinations of polymers of synthetic and natural origin are widely used. The combination of polylactide and chitosan has led to the development of scaffolds for bone tissue engineering [19]. Additionally, the addition of polyvinyl alcohol to other natural polymers leads to the formation of hybrid materials with enhanced mechanical properties [20,21].

However, in addition to combining the properties of various polymers in the development of new hybrid materials, it is also currently of interest to study the influence of various physico-mechanical factors affecting the properties of polymers and, subsequently, materials based on them. Physico-mechanical factors contribute to the improvement of the microstructure, lead to the formation of free radicals (hydrogen, hydroxyl and others), contribute to the formation of materials with a certain polymer molecular weight distribution, contribute to the formation of intermolecular crosslinks, make it possible to obtain materials with a hierarchical porous structure, and in some cases cause improvement in the antibacterial activity of polymeric materials [22–27]. The literature contains reports on the use of the following physical and mechanical factors that affect the properties of polymers and other materials during their freezing and subsequent freeze-drying as the main stages in the production of highly porous polymeric materials [28,29]: high-pressure expansion, radiofrequency treatment, the use of electric and magnetic fields and ultrasonic treatment. These physical and mechanical factors contribute to the formation of smaller ice crystals during the freezing of polymer solutions, which subsequently affects the quality and microstructure of materials after the freeze-drying process [30].

However, from the above range of physical and mechanical factors, the most promising, in terms of minimizing material and energy costs, is the use of ultrasound. First, in contrast to the high-pressure expansion method, the impact of ultrasound on polymer solutions (in particular, ultrasonic freezing) does not require the presence of compression units [28]. Secondly, in contrast to the impact of electric and magnetic fields, the contact of foreign elements directly with the solution is not required, and the transmission of ultrasonic exposure is carried out by creating acoustic pressure on the wall of the container containing the solution due to vibrations produced by the piezoelectric element [30]. Thirdly, during ultrasonic treatment (in particular, ultrasonic freezing), surface stresses are created in capillaries, as a result of which microchannels are formed that facilitate easier removal of moisture from the material during subsequent freeze-drying [31]. During ultrasonic treatment of polymer solutions under the action of external pressure, microbubbles filled with gas vibrate—this phenomenon is called acoustic cavitation. When the cavitation bubbles collapse, the solvent molecules (water) inside them can dissociate with the formation of radicals. In the case of water, hydroxyl radicals (OH radicals) and hydrogen atoms are formed. Some of these radicals diffuse from the cavity of the bubble into the surrounding liquid, where they can react with molecules of the solute (polymer). Induced OH-radical processes can lead to polymer degradation; however, it is noted in [24] that this can also initiate intermolecular cross-linking of polymers.

As noted above, one of the stages in the production of polymer matrices for cell cultivation is vacuum freeze-drying. The conditions of the drying process (vacuum 10–100 Pa and low temperature  $-50\text{ }^{\circ}\text{C}$ ) contribute to the formation of a highly porous structure with minimal shrinkage of the material. This technological process is divided into several main stages: preliminary freezing and the first and second drying periods. In our previous study [32], we considered the effect of ultrasound on the freezing kinetics of polymers of various natures and the size distribution of ice crystals. However, the study, analysis and comparison of a set of properties of polysaccharides and materials based on them, subjected to physical and mechanical influences in the stage of preliminary freezing, is also an urgent task.

In [33], a classification of ultrasonic waves depending on frequency and power is given. In accordance with this classification, ultrasonic waves in the range from 20 to 100 kHz are defined as “powerful ultrasound”. These ultrasonic waves, at a high power level (several tens of watts), are able to act on the medium in which they propagate and modify it as a result of the occurrence of acoustic cavitation, leading to macroscopic effects. Therefore, powerful ultrasound is widely used in sonochemistry and is also used to intensify heat and mass transfer processes. On the contrary, low-power ultrasound (<10 W) in the frequency range above 1 MHz is mainly used in medical diagnostics and does not affect the propagation medium. Therefore, in the present study, ultrasound with a frequency of 40 kHz and a power of 50 W was chosen as a physical and mechanical factor affecting the microstructure of polysaccharides and materials based on them. Ultrasound with these characteristics under pulsed action can affect the structure of ice crystals in polysaccharide solutions and does not lead to the melting of samples in the freezing stage.

The use of ultrasound during the stage of freezing materials allows one to influence the shape of ice crystals and their direction; in accordance with this, materials of anisotropic shape can be obtained. Ultrasound is also capable of acting on the vibrational spectra of molecules and intensifying heat and mass transfer at the freezing stage [32]. The study of these aspects can contribute to the development of both theoretical and practical knowledge about the relationship between the structure and properties of the obtained materials, as well as accelerate the development of materials with different structure and direction of pores and expand their areas of application. Therefore, the purpose of this work was to study the effect of ultrasound applied during the stage of preliminary freezing of solutions of polysaccharides and materials based on them, specifically on a set of their properties, namely: microstructure, vibrational spectra of molecules, porosity, sorption capacity, permeability of the porous structure of materials and the subsequent possibility of culturing cells in the developed polymer scaffolds.

## 2. Materials and Methods

### 2.1. Materials and Reagents Used

The following polymers and auxiliary reagents were used in the work: sodium alginate (RusChem, Moscow, Russia), low-molecular-weight chitosan with a deacetylation degree of more than 75% and a molecular weight of 314 kDa (Sigma-Aldrich, Saint Louis, MO, USA), edible gelatin and agar (B&V srl, Parma, Italy). Distilled water was used as a solvent. Separately, distilled water acidified with glacial acetic acid (RusChem, Moscow, Russia) was used to dissolve the chitosan.

### 2.2. Method for Obtaining Solutions of Polysaccharides and Matrices Based on Them

The objects of study were individual polysaccharides: sodium alginate (Alg) and chitosan (Ch), as well as polymer matrices developed on their basis for cell cultivation. The first matrix is a crosslinked polyelectrolyte complex, alginate–chitosan (Alg–Ch). Sodium alginate and chitosan are widely used in tissue engineering for culturing mammalian cells; however, these polymers do not contain cell recognition sites, the Arg–Gly–Asp (RGD-peptide) sequences that promote cell adhesion and proliferation. Therefore, when developing the second matrix, it was decided to mix a polysaccharide, sodium alginate, with a polymer of protein origin, gelatin, since gelatin contains RGD sequences in its structure [34]. Thus, the second composite was obtained, an alginate–gelatin matrix (Alg–G), with the addition of agar. Agar acts as a substance that increases the structural integrity of the matrix due to its increased ability to form stable gels.

The stages of polymeric material preparation are shown in Figure 1. Alg 1.5% and Ch 1% were used to form the cross-linked polyelectrolyte complex Alg–Ch with polymer concentrations of 1.5 and 1% for Alg and Ch, respectively. Alg 1.5% and Ch 1.5%, with a polymer volume ratio of 1:1, were supplemented with 0.5% agar solution to form Alg–G, kept for one hour at 50 °C and pre-chilled in a refrigerator at 4 °C (Figure 1a). Distilled water acidified with glacial acetic acid (pH = 4) was used to dissolve the Ch. The resulting

polymer solutions were poured into Petri dishes so that the layer thickness was 0.003 m. This sample layer thickness was chosen for the following reasons: First, at a large thickness of the solution layer, the freezing rate gradient can lead to the formation of ice crystals of various sizes in the axial section. Secondly, the upper layer of the solution, located farther from the source of ultrasonic vibrations, may not be subjected to ultrasonic action.

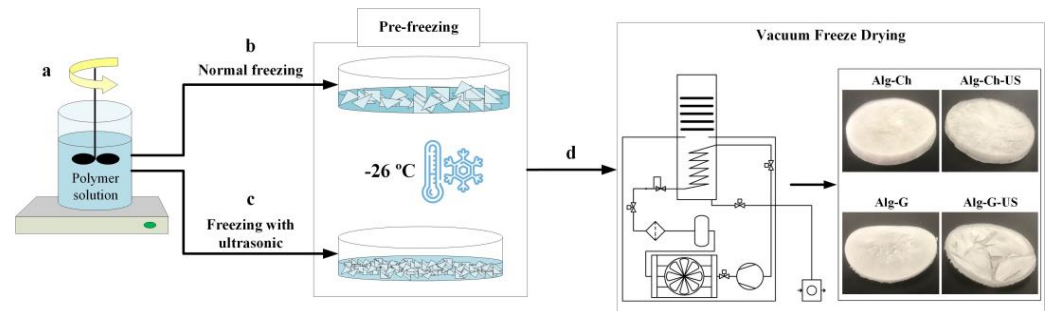


**Figure 1.** The stages of polymeric material preparation: preparation of polymer solutions (a), pre-freezing (conventional freezing (b) or freezing with ultrasound (c)), vacuum freeze-drying (d).

The first part of the test samples, placed in Petri dishes, was frozen in a quick freezer without exposure to ultrasound at a temperature of  $-26\text{ }^{\circ}\text{C}$  (Figure 1b). The second part of the samples was also frozen at  $-26\text{ }^{\circ}\text{C}$ ; however, at the phase transition stage, which was monitored using thermocouple readings, the studied polymer solutions were exposed to ultrasound at a frequency of 40 kHz and a power of 50 W (Figure 1c). To implement freezing with the use of ultrasound, an installation was assembled that allows the sonocrystallization process to be carried out to obtain smaller and more uniform ice crystals in the polymers under study. A detailed description of the installation and the mode of ultrasonic freezing were presented in our previous study [32]. Therefore, these aspects will not be presented in detail in this paper.

Eight samples were obtained, and their full specification is given in Table 1.

**Table 1.** Complete list of received samples.

No.	Polymers	Concentration, %	Sonication
Alg	Sodium alginate	1.5	–
Alg-US	Sodium alginate	1.5	+
Ch	Chitosan	1	–
Ch-US	Chitosan	1	+
Alg-Ch	Alginate–chitosan	1.5 and 1 (1:1)	–
Alg-Ch-US	Alginate–chitosan	1.5 and 1 (1:1)	+
Alg-G	Alginate–gelatin	1.5 and 1.5 (1:1)	–
Alg-G-US	Alginate–gelatin	1.5 and 1.5 (1:1)	+

In the final stage in vacuum freeze-drying (Figure 1d), an “ice-steam” phase transition takes place that occurs at certain temperature and pressure parameters (below 611 Pa and  $0\text{ }^{\circ}\text{C}$ ). Such process conditions ensure the preservation of the shape of the material and contribute to the formation of its macroporous structure.

To implement the process of vacuum freeze-drying, a mode was chosen in which the temperature of the shelves changed over time stepwise according to the task. The pressure in the working chamber was 68 Pa. Table 2 shows the temperature and time parameters for this drying mode.

**Table 2.** Temperature and time parameters of freeze-drying.

Temperature and Time Parameters				
$T_{\text{shelf}},\text{ }^{\circ}\text{C}$	0	5	10	20
Time, h	0–8	8–13	13–19	19–25

A detailed description of the analytical studies of the samples, their comparison and analysis are presented below.

### 2.3. Infrared Spectroscopy (IR Spectroscopy)

To study the effect of ultrasound (US) on chemical bonds in the studied polysaccharides and their mixtures (changes in the vibrational spectra of molecules), we used the IR spectroscopy method, which was carried out for samples in liquid form. For this, the following samples (solutions of polysaccharides) were prepared, information on which is given in Table 3.

**Table 3.** Specifications for IR spectroscopy.

No.	Without US	No.	US Parameters		No.	US Parameters	
			$f$ , kHz	$P_r$ , W		$f$ , kHz	$P_r$ , W
Alg	Control	Alg-US	40	50	Alg-US-I	40	90
Ch	Control	Ch-US	40	50	Ch-US-I	40	90
Alg-Ch	Control	Alg-Ch-US	40	50	Alg-Ch-US-I	40	90

The first part of the samples (control) was not treated with ultrasound and was used to compare and determine the effect of ultrasound parameters on the vibrational spectra of molecules. The second part of the samples was treated with ultrasound at a frequency ( $f$ ) 40 kHz and a power ( $P_r$ ) 50 W for 20 min. To determine the effect of power and intensity of ultrasound on the vibrational spectra of molecules, a third of the samples were also treated with ultrasound for 20 min at a frequency ( $f$ ) of 40 kHz and a power ( $P_r$ ) of 90 W.

This study was carried out using a Nicolet 380 IR-Fourier spectrometer (Thermo Fisher Scientific Inc., Waltham, MA, USA). The following spectral range was used in the work: 500–4000  $\text{cm}^{-1}$ . An analytical study was carried out at the Center for Collective Use of the MUCTR.

### 2.4. Study of the Structure of Ice Crystals

To study the structure and analyze the effect of ultrasound on the morphology of ice crystals formed during the freezing of polymer solutions, an Olympus CX 41 light microscope with a camera and a PE 120 cooling stage (limiting cooling temperature  $-18\text{ }^\circ\text{C}$ ) was used. A detailed description of the research methodology was presented in our previous work [32].

### 2.5. Scanning Electron Microscopy (SEM)

To visualize, study, analyze and compare the surface morphology of Alg-Ch and Alg-Ch-US samples in cross-section, a JEOL 1610LV scanning electron microscope (JEOL, Tokyo, Japan) was used. An analytical study was carried out at the Center for Collective Use of the MUCTR. For all other samples, a VEGA3 TESCAN scanning electron microscope (TESCAN, Brno-Kohoutovice, Czech Republic) was used. An analytical study was carried out at the Department of Chemistry and Technology of Crystals of the MUCTR.

### 2.6. Sample Porosity Study

To determine the true density and subsequent calculation of the porosity of the studied polymeric materials, an Accu Pyc 1340 automatic helium pycnometer (Micromeritics Instrument Corp., Norcross, GA, USA) was used. An analytical study was carried out at the Center for Collective Use of the MUCTR.

### 2.7. Study of the Sorption Capacity of Samples

Sorption capacity is one of the functional characteristics of polymeric materials that depends on the pore volume and is determined by the amount of liquid that 1 g of dry material can absorb.

To measure the sorption capacity, the mass of dry samples was first determined on an analytical balance. Then, 10 mL of water at room temperature was added to pre-weighed samples and left for 10 min. After the time had elapsed, the samples were removed from the water and weighed again on an analytical balance. After that, the samples were immersed in water for another 10 min to determine the value of the sorption capacity after 20 min. Upon completion of the experiment, the value of the sorption capacity ( $\omega$ ) of the samples was calculated using the formula below:

$$\omega = \frac{m_2 - m_1}{m_1}, \quad (1)$$

where  $m_1$ —the mass of dry material, g and  $m_2$ —the mass of the material that has absorbed water, g.

### 2.8. Study of the Permeability of the Porous Structure

The permeability of the porous structure is an important characteristic for materials used in the field of cell culture. The permeability of the porous structure determines the amount of incoming oxygen and nutrients necessary for culturing cells in matrices. The presence of microchannels in a porous structure can contribute to the active mass transfer of oxygen and essential nutrients that promote cell growth and development. To study the permeability, methylene blue dye, previously diluted in 60% ethanol, was introduced into the Alg-Ch, Alg-Ch-US, Alg-G, and Alg-G-US polymer matrices using a thin needle. To visualize dye diffusion through the porous structure of matrices, an ADF S645 stereomicroscope (ADF Optics Co Ltd., Zhejiang, China) was used.

### 2.9. Study of the Permeability of the Porous Structure

A test for antibacterial activity was carried out for the samples, which included chitosan, in order to establish the bactericidal properties of these samples. To test for antibacterial activity, LB agar nutrient medium was added to Petri dishes with a diameter of 90 mm, on the surface of which a layer of culture of the studied pathogenic bacteria was sown: *Escherichia coli*, *Pseudomonas aeruginosa*, *Staphylococcus aureus* or *Bacillus cereus*. During the experiment, 0.1 mL of a suspension of microorganisms was applied at a concentration of  $1.5 \times 10^9 \text{ mL}^{-1}$  cells in the active growth phase and evenly distributed with a sterile spatula over the surface of the nutrient medium. Then, the investigated samples of polymeric materials were added to the surface of the nutrient medium: Ch, Ch-US, Alg-Ch and Alg-Ch-US. Cultivation was carried out at 37 °C for 24 h.

The result of the analysis of antibacterial activity was the zone of inhibition of the growth of pathogenic bacteria, i.e., a zone free from microorganisms, the size (thickness) of which was determined as shown in Figure 2.

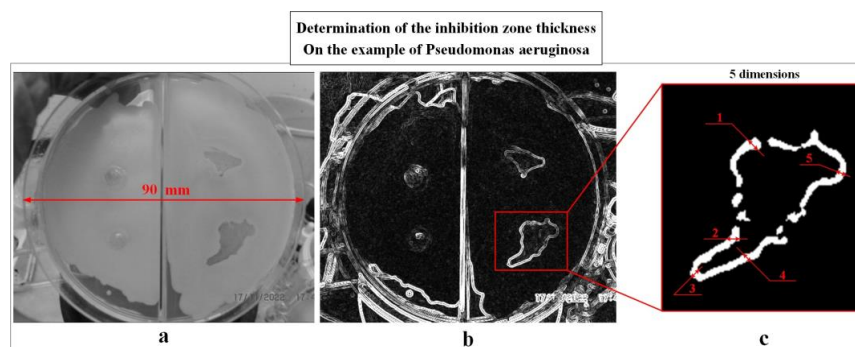


**Figure 2.** Steps for measuring the thickness of the inhibition zone: setting the scale according to the diameter of the Petri dish (a), highlighting the area (b) and performing five measurements (1–5) along the perimeter of the zone of inhibition (c).

In the first stage, the ratio between the scale and pixels of the image was determined by the known diameter of the Petri dish (Figure 2a). Then the image was converted to an 8-bit format and an automatic search for the boundaries of objects was performed (Figure 2b), after which five measurements of the thickness of the inhibition zone were made for each sample (Figure 2c). An analytical study was carried out at the Department of Biotechnology of the MUCTR.

#### 2.10. Test for Degradation of Matrices in the Culture Medium DMEM

Samples of Alg-Ch, Alg-Ch-US, Alg-G and Alg-G-US were previously tested for degradation in DMEM culture medium containing 1 g/L glucose and glutamine. For this purpose, Alg-Ch, Alg-Ch-US, Alg-G, and Alg-G-US samples with initial weights of 0.0417, 0.0387, 0.0188, and 0.0219 g, respectively, were placed in Petri dishes, poured into 10 mL of DMEM medium, and kept at a temperature of 37 °C. Changes in the mass of samples and the pH of the culture medium were recorded every 24 h for three days. According to the results of the experiment, the possibility of cultivating cells in the obtained matrices was established.

#### 2.11. Cultivation of Fibroblast Cells in Matrices

The source of fibroblasts was the epididymal fat of B10.GFP mice. Cultivation was carried out in DMEM supplemented with 10% fetal bovine serum (FBS) (Himedia, Maharashtra, India, RM10432), 100x GlutaMAX (Gibco, Thermo Fisher Scientific Inc., Waltham, MA, USA, 35050038), 10 ng/mL basic fibroblast growth factor (bFGF) and 1% insulin–transferrin–selenite (PanEco, Moscow, Russia, F065), under standard incubation conditions at 37 °C and 5% CO<sub>2</sub>.

The studied matrices based on alginate–chitosan and alginate–gelatin were sterilized using ultraviolet irradiation for two hours. The sterilized samples were then transferred to the Federal Scientific and Clinical Center for Physicochemical Medicine named after Academician Yu.M. Lopukhin for research on the cultivation of fibroblast cells in matrices.

The test matrices were placed on the bottom of a 96-well plate (Costar, Corning, Cambridge, MA, USA, 3599) using sterile tweezers, and 50 µL of culture medium was applied on top. At the same time, the cells of the ninth passage were washed three times from the medium using a Versene solution (PanEco, Moscow, Russia, P080p), and then removed from the T75 flasks (SPL Life Sciences, Pocheon-si, Gyeonggi-do, Republic of Korea, 70075) using 5 mL of a solution of 0.25% trypsin and 0.02% EDTA in Dulbecco's phosphate-buffered saline (DPBS) (Himedia, Maharashtra, India, TCL007). After complete detachment, the cells in suspension were transferred to a 15 mL centrifuge tube with 4 mL of F12 medium (PanEco, Moscow, Russia) with 10% FBS for detrypsinization, and the cells were counted with trypan blue in a Luna II automatic counter (Logos Biosystems, Dongan-gu Anyang-si, Gyeonggi-do, Republic of Korea, L40002, L12002) and then centrifuged at 200 rcf for 5 min in a Centrifuge 5804R centrifuge (Eppendorf, Hamburg, Germany, 5805000010). Next, the supernatant was taken, the cell culture medium was added to the cell sediment and resuspended, and the cells were seeded on matrices at a density of 5000/well. The plate was then left in an incubator at 37 °C and 5% CO<sub>2</sub> for 24 h.

Twenty-four hours after seeding, cell morphology was analyzed on matrices using an Olympus IX53F fluorescence microscope with 4 fluorescence filters (Olympus, Tokyo, Japan) using CellSens Standart morphometry software.

To test for cell viability, 10 µL of PrestoBlue cell viability indicator (Thermo Fisher Scientific Inc., Waltham, MA, USA) was added to the wells of a 96-well plate with matrices, cells, and 100 µL of growth medium and incubated at 37 °C and 5% CO<sub>2</sub> for 4 h. The analysis of the results was carried out using an Infinite 200 Pro multi-mode reader model Infinite M Plex-Tecan (Tecan, Mennedorf Switzerland, 30190085) and I-control software at  $\lambda_{\text{ex}} = 560 \text{ nm}$ ,  $\lambda_{\text{em}} = 590 \text{ nm}$ .

In parallel, a comparison experiment was carried out in which fibroblast cells were seeded on plastic in order to determine the adhesion strength of cells to matrices.

### 3. Results and Discussion

#### 3.1. Results of IR Spectroscopy

To study the effect of ultrasounds of different power and the same frequency (40 kHz) on the vibrational spectra of the polysaccharide molecules sodium alginate, chitosan and chitosan alginate, IR spectra were obtained, shown in Figure 3.

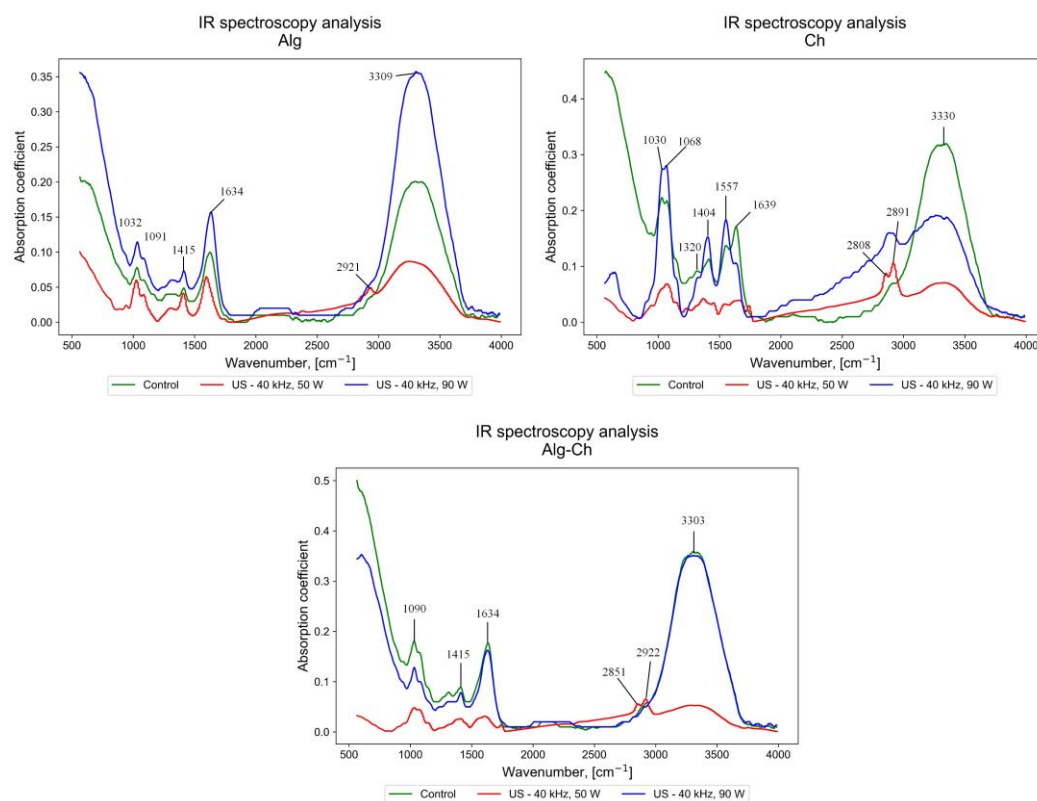


**Figure 3.** Results of IR spectroscopy for the studied polysaccharides.

An analysis of the results of IR spectroscopy for sodium alginate made it possible to determine that, compared with the control sample (Alg), the Alg-US-I sample treated with ultrasound with a power of 90 W had increased stretching vibrations in its  $-OH$  bonds ( $3309\text{ cm}^{-1}$ ), stretching asymmetric and symmetric vibrations of the carboxyl ion ( $1634$  and  $1415\text{ cm}^{-1}$ ), and C-O stretching vibrations and bending vibrations in its C-O-H ( $1091\text{ cm}^{-1}$ ) and C-C-H bonds ( $1032\text{ cm}^{-1}$ ) [35]. At the same time, the Alg-US sample treated with ultrasound with a power of 50 W shows a decrease in the absorption coefficient for the above bonds compared with the control sample (Alg). However, for Alg-US, a pronounced stretching vibration of the aliphatic bond  $-CH$  ( $2921\text{ cm}^{-1}$ ) is observed.

For chitosan, it was determined that, compared with the control sample (Ch), in the Ch-US and Ch-US-I samples, the stretching vibrations of  $-OH$  bonds and  $-NH_2$  (in the region of  $3330\text{ cm}^{-1}$ ) decrease, while the stretching vibrations of  $-CH$  bonds and  $-OH$  in the region from  $2750$  to  $3000\text{ cm}^{-1}$  increase, with Ch-US-I to a greater extent than Ch-US. In the Ch-US sample, compared to Ch-US-I, there is a fragmentation of two peaks:  $-OH$  ( $2891\text{ cm}^{-1}$ ) and  $-CH$  ( $2808\text{ cm}^{-1}$ ). The peaks at  $1030$  and  $1068\text{ cm}^{-1}$  refer to C-O stretching and C-O-C stretching in the glucopyranose ring, respectively, with a higher absorption coefficient for the Ch-US-I sample. The peaks at  $1320$  and  $1404\text{ cm}^{-1}$  are related to the absorption of C-N  $CH_3CONH$  (amide III) and the symmetrical deformation of  $CH_2$  as well as  $CH_3$  [13,36] and are enhanced for Ch-US-I. The peaks at  $1639$  and  $1557\text{ cm}^{-1}$  due to the  $-CONH_2$  stretching vibration were enhanced for Ch-US-I and significantly attenuated for Ch-US compared to Ch.

The IR spectra for the alginate–chitosan binary mixture were also analyzed. The broad peak obtained in the range of  $3303\text{ cm}^{-1}$  indicates the presence of  $-\text{OH}$  stretching, polymer association, and intermolecular hydrogen bonds in the alginate–chitosan binary mixture, which are equivalent for the Alg-Ch and Alg-Ch-US-I samples. The peaks at  $2922$ ,  $2851$ ,  $1634$ ,  $1415$  and  $1090\text{ cm}^{-1}$  show the presence of an asymmetric stretch  $-\text{CH}$ , a symmetric stretch  $-\text{CH}$ , a carbonyl group, an  $-\text{NH}$  bend (amide II band) and a  $-\text{CH}$  deformation (split peaks in  $\text{CH}_2$  and  $\text{CH}_3$ , respectively) [37]. The IR spectra show that the carboxylated group of the alginate was dissociated into a  $\text{COO}^-$  group, which forms a complex with the protonated amino group of chitosan through electrostatic interaction. As the mixture is formed, hydrogen bonds are formed due to an increase in intermolecular attraction between alginate and chitosan.

### 3.2. Results of Microscopic Examination of Ice Crystals

In the course of the work, microphotographs of ice crystals were obtained for the studied solutions of polysaccharides, treated and not treated with ultrasound (40 kHz, 50 W) during the freezing stage, at magnifications of 200 and 50  $\mu\text{m}$ . The results obtained are presented in Figure 4.

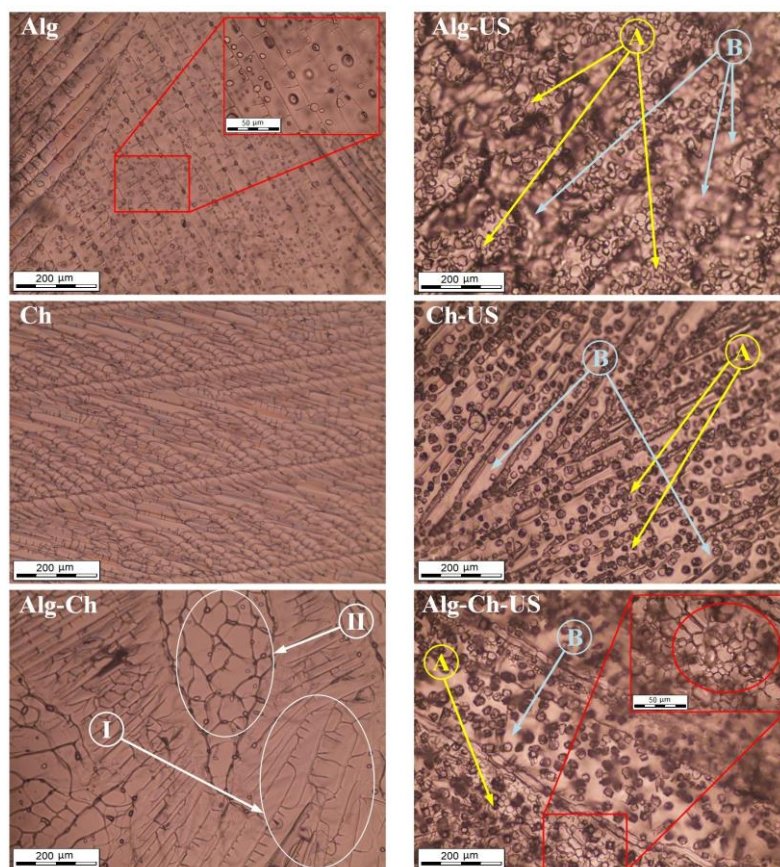


**Figure 4.** Microphotographs of ice crystals for the studied polysaccharides: overlay textures of alginate (I) and chitosan (II) separately; accumulation of small ice crystals (A); microchanneling (B).

The use of ultrasound at the phase transition stage in the freezing process made it possible to reduce the size of the resulting ice crystals for all the polymers under study. The micrographs of the Alg-US, Ch-US and Alg-Ch-US samples show zones with a large accumulation of small ice crystals (Figure 4A), as well as zones free of ice crystals (Figure 4B). Zones free from ice crystals are microchannels, which, during subsequent freeze-drying, contribute to the active mass transfer of moisture. The even distribution of ice crystals can affect the porosity and hence the sorption capacity of the materials obtained after drying.

In addition, the structuring of ice crystals in frozen polysaccharides during subsequent vacuum freeze-drying promotes the formation of channels in the axial section, which can favorably affect the diffusion of oxygen entering the polymer framework at the stage of cell cultivation.

### 3.3. Surface Morphology Results

In the course of the experimental work, scanning electron microscopy images were obtained for conventional matrices based on alginate–chitosan and alginate–gelatin as well as for matrices of identical composition treated with ultrasound during the freezing of the initial solutions. The images obtained using scanning electron microscopy made it possible to analyze the effect of ultrasound (40 kHz, 50 W) on the surface morphology of the samples under study.

Dried Alg-Ch and Alg-Ch-US cylindrical samples were cut with a thin blade in the transverse section (top view) and in axial section (front view) for a comprehensive study of the effect of ultrasound on the surface morphology of materials. The obtained SEM images of the matrices based on alginate–chitosan in various sections are shown in Figure 5.

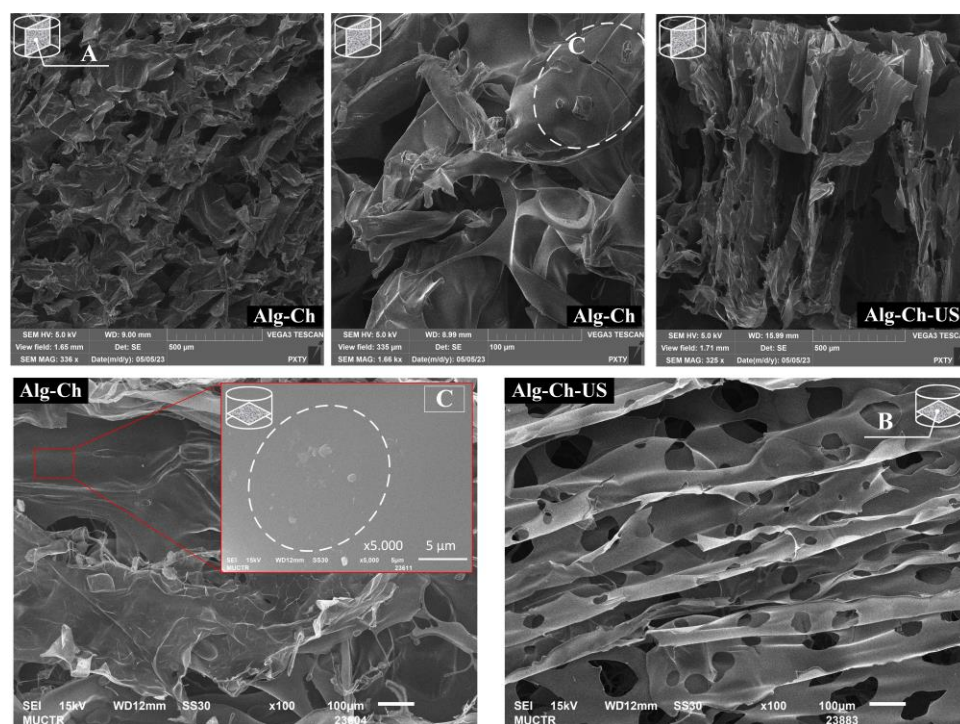


**Figure 5.** Surface morphology of matrices based on alginate–chitosan: axial section or front view (A), cross section or top view (B), supramolecular formation of a granular structure characteristic of chitosan (C).

An analysis of the SEM images showed that the Alg-Ch samples have an irregular lamellar structure of the alginate component, with a plate thickness of up to 3 µm. When comparing SEM images of Alg-Ch and Alg-Ch-US samples in axial section, it can be seen that ultrasound contributed to the structuring of the alginate component plates in a vertical position, which corresponds to the direction of ultrasonic waves and, accordingly, acoustic pressure. The samples also show supramolecular granular structures characteristic of chitosan (Figure 5C), which was detailed in [14].

When comparing cross-sectional SEM images, it can be seen that ultrasound contributed to a uniform distribution of pore sizes, which correlates with the data obtained from microscopic examination of ice crystals (Figure 4). The average pore size of the Alg-Ch sample was 160 µm, and the minimum and maximum sizes were 70 and 250 µm,

respectively, while for Alg-Ch-US, the average pore size was 71  $\mu\text{m}$ , and the minimum and maximum sizes were 15 and 155  $\mu\text{m}$ , respectively.

The obtained SEM images of matrices based on alginate–gelatin in axial and cross sections are shown in Figures 6 and 7, respectively.

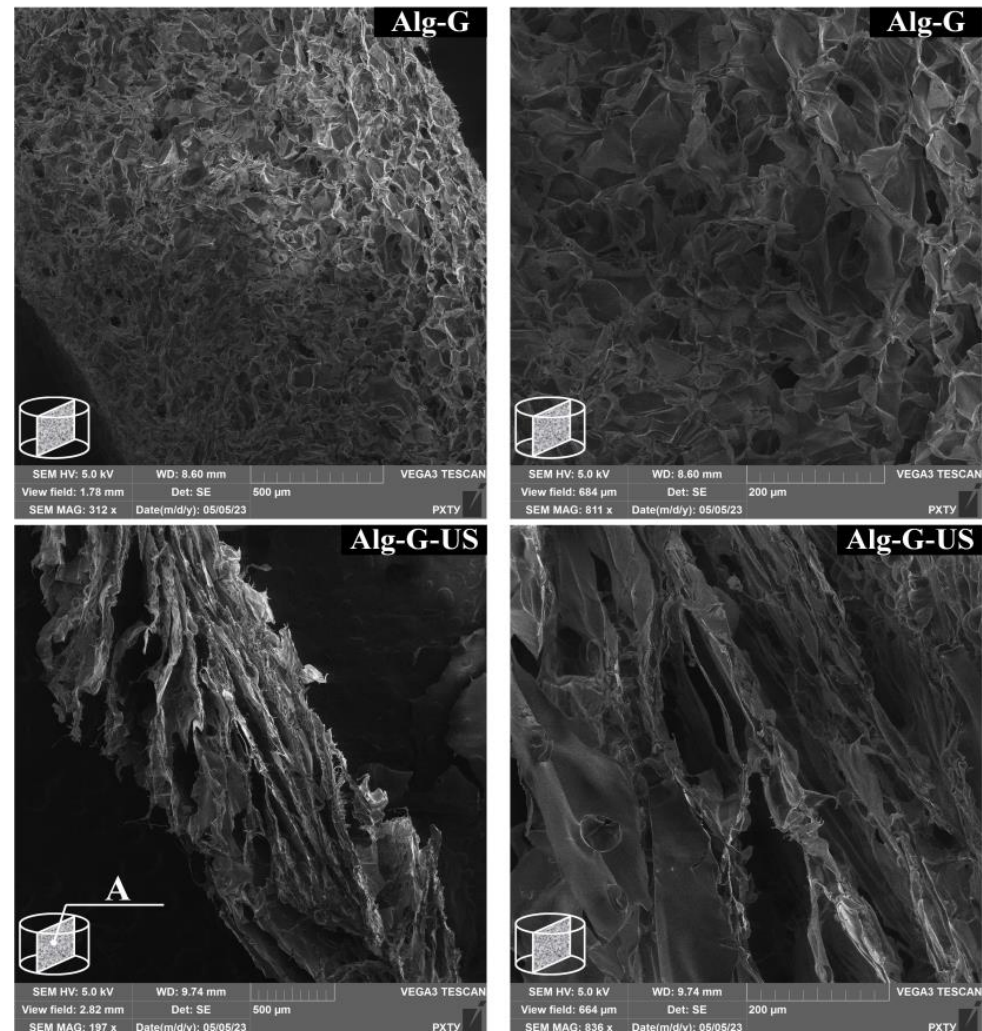


**Figure 6.** Surface morphology of alginate–gelatin matrices: axial section or front view (A).

The analysis of the SEM images showed that the Alg-G sample has a dense cellular structure in both sections (Figures 6 and 7B), which is consistent with the data presented in [38,39]. Meanwhile, in the Alg-G-US sample, both sections are dominated by hollow plates structured in the direction of ultrasound action, with a wall thickness of up to 2  $\mu\text{m}$ .

The SEM images of the Alg-G-US sample (Figure 7C) show fibrous formations up to 1.5  $\mu\text{m}$  thick and up to 25  $\mu\text{m}$  high, which are not characteristic of the Alg-G sample, and the formation of which can be attributed to sonication.

In the Alg-G-US sample, elongated, oval structures were observed, in the center of which there were 7.5  $\mu\text{m}$  cavities (Figure 7D). The presence of these can be associated with the formation and collapse of cavitation bubbles during sonication.

It should be noted that the average pore size of the Alg-G sample was 35  $\mu\text{m}$ , which is significantly smaller than that of the Alg-Ch sample.

At present, the effect of ultrasound on the directionality of the porous structure in polysaccharide materials is practically not presented in the literature; therefore, the data obtained (Sections 3.2 and 3.3) make an important practical and theoretical contribution to

the development of the field of development of polysaccharide matrices with an anisotropic (directional) porous structure.

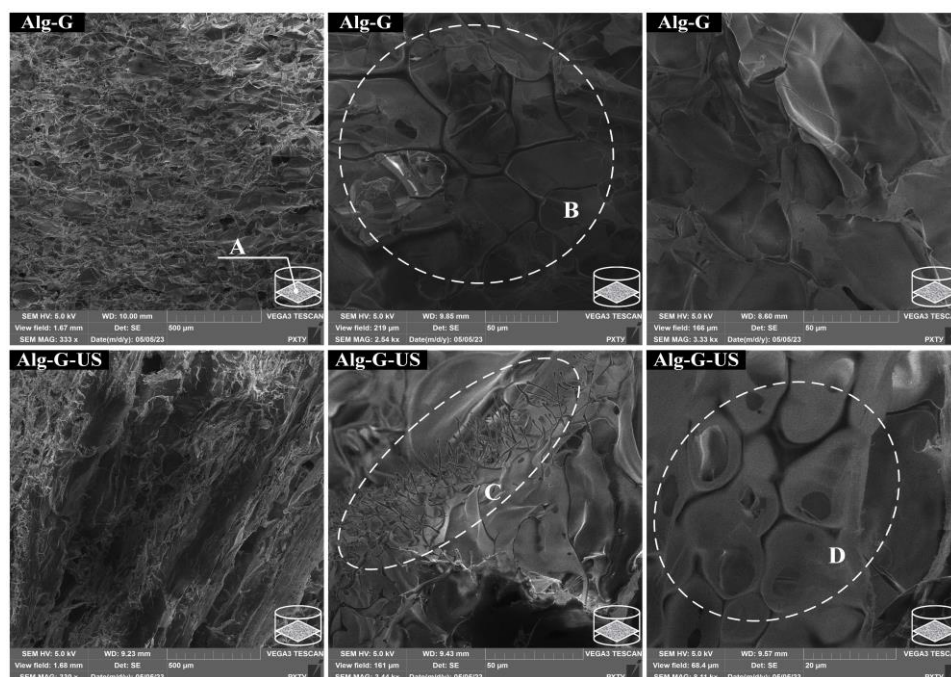


**Figure 7.** Surface morphology of alginate–gelatin matrices: cross section or top view (A), cellular structure (B), fibrous formations (C), oval structures with cavities in the center (D).

### 3.4. The Results of the Study of Porosity and Sorption Capacity of Samples

To study the effect of ultrasound (40 kHz, 50 W) on the porosity of polysaccharides, data on the true density of sodium alginate and chitosan, as well as a matrix based on alginate–chitosan, dried by vacuum freeze-drying, were obtained using a helium pycnometer. The values of the apparent density of the investigated samples of cylindrical shape were determined by measuring the mass of the samples and determining the volume of the samples by measuring the characteristic dimensions of the cylinder (height and diameter) using an electronic caliper in triplicate for each sample. The experimental data obtained during the work are presented in Table 4.

**Table 4.** Values of true and apparent density of materials.

No.	$\rho_{bulk}$ , g/cm <sup>3</sup>	$\rho_{apparent}$ , g/cm <sup>3</sup>	$V_{por}$ , cm <sup>3</sup>
Alg	0.042	1.74	23.3
Alg-US	0.029	1.75	33.1
Ch	0.018	1.77	56.2
Ch-US	0.023	1.54	43.2
Alg-Ch	0.024	1.62	40.5
Alg-Ch-US	0.023	1.75	43.1

Based on the obtained data on the true and apparent density, the porosity of the samples was calculated using the following equation:

$$\varphi = 1 - \frac{\rho_{bulk}}{\rho_{apparent}}, \quad (2)$$

where  $\varphi$ —porosity;  $\rho_{bulk}$ —apparent density, g/cm<sup>3</sup>;  $\rho_{apparent}$ —true density, g/cm<sup>3</sup>.

According to the results of the porosity calculation for the studied samples, a diagram was built, shown in Figure 8A. Based on the obtained data on porosity and apparent density, the pore volume  $V_{por}$ , shown in Table 4, was calculated using the following equation:

$$V_{por} = \frac{\varphi}{\rho_{bilk}}, \quad (3)$$

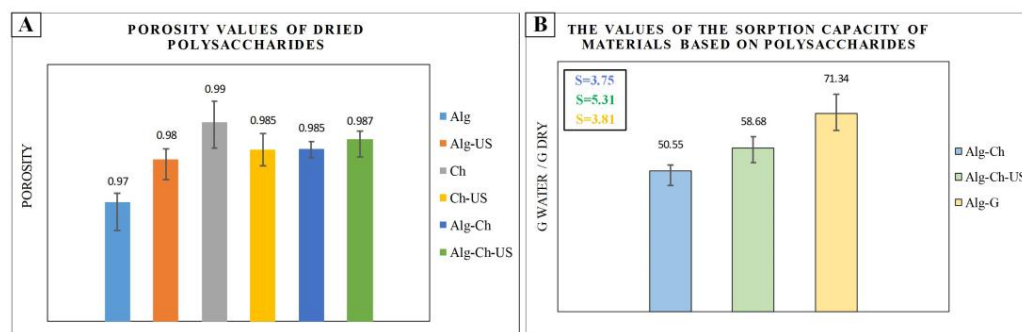


**Figure 8.** Diagrams of porosity (A) and sorption capacity (B) of obtained samples.

The sorption capacity of materials depends on the pore volume. The sorption capacity was measured for the cross-linked matrices Alg-Ch, Alg-Ch-US and Alg-G, but the Alg-G-US sample did not pass the sorption capacity test, because it lost structural integrity due to the presence of wide channels in the axial section formed during sonication. The obtained values of sorption capacity as well as the values of the standard deviation are shown in the diagram (Figure 8B).

The standard deviation was estimated using Equations (4) and (5). First, the arithmetic mean of the sample  $\bar{x}$  was determined using Equation (4):

$$\bar{x} = \frac{1}{n} \sum_{i=1}^n x_i, \quad (4)$$

where  $n$  is the selection size;  $x$ —selection element;  $i$  is the number of the selection element.

Then, the standard deviation  $S$  was calculated using Equation (5):

$$S = \sqrt{\frac{1}{n} \sum_{i=1}^n (x_i - \bar{x})^2}, \quad (5)$$

The studied samples showed high values of porosity, (>90%), which coincides with the data presented in [40]. For samples treated with ultrasound, the porosity values did not differ significantly. However, the pore volume of the sonicated samples was higher than that of the conventional samples (Table 4).

The sorption capacity dependent on pore volume was higher for the sample with large pore volume, namely Alg-Ch-US, compared to Alg-Ch. The higher sorption capacity for the Alg-G sample compared to the Alg-Ch sample can be attributed both to the nature of its constituent polymers and to the higher porosity of the Alg-G sample, as shown in the SEM images in Section 3.3. The Alg-G sample is more swellable than Alg-Ch, as it contains sodium alginate and gelatin, which have a high degree of swelling and the ability to actively absorb liquid.

### 3.5. The Results of the Study of the Permeability of the Porous Structure

The study of the permeability of the porous structure of the resulting matrices is an important task in the field of cell cultivation as the permeability of the porous structure affects the amount of incoming oxygen and nutrients necessary for culturing cells in matrices.

The results of the study of the permeability of the porous structure for the obtained samples in various sections are shown in Figure 9.

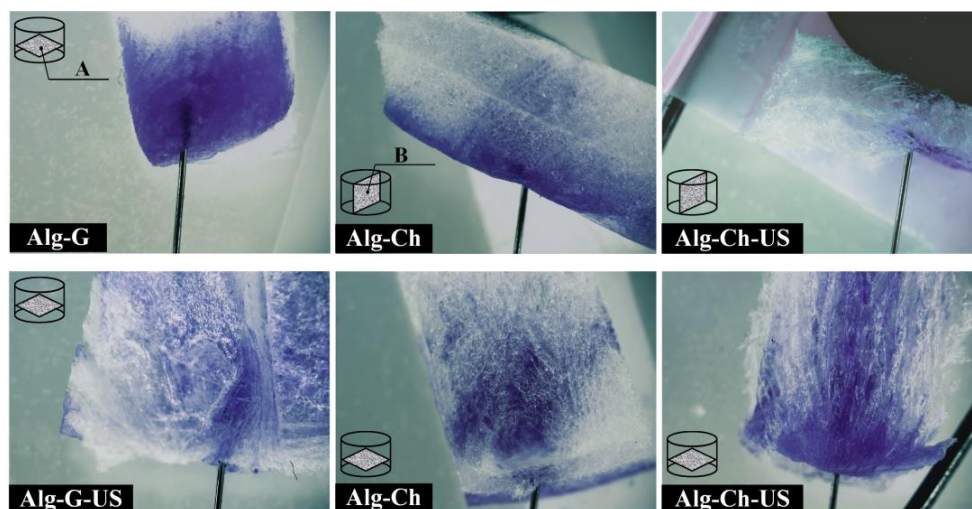


**Figure 9.** The results of the study of the permeability of the porous structure of the samples: cross section or top view (A), axial section or front view (B).

The sorption rate depends on the nature of the polymers that make up the materials. Alg-G and Alg-G-US matrices contain both sodium alginate and gelatin, which have a high swelling capacity; therefore, the diffusion of colored alcohol proceeded faster in these samples compared to samples based on alginate–chitosan. When analyzing the Alg-G-US sample, it was seen that the presence of rather wide transverse channels prevented the passage of liquid into the layer of material due to the low pressure in the channel; however, the liquid quickly diffused into the lateral regions of the material, which also had channels (smaller) in axial section.

The rate of diffusion of colored alcohol in the Alg-Ch and Alg-Ch-US samples was slower compared to the Alg-G and Alg-G-US samples. In the Alg-Ch sample, stagnant zones were observed in the axial section; the main part of the dye accumulated near the surface of the matrix. Part of the tinted alcohol, which has a high speed and, accordingly, pressure in the area of its introduction, passed into the thickness of the Alg-Ch sample, corresponding to the direction of the introduction of the dye.

For the Alg-Ch-US sample in the axial section, similarly to the Alg-G-US sample, a decrease in the speed of colored alcohol was observed in the region where large channels appeared; however, the dye passed through the formed channels. In this case, similarly to the Alg-Ch sample, the accumulation of the dye near the surface of the sample was observed.

For the Alg-Ch-US sample in cross section, the highest speed of dye movement was observed in the area of its introduction. In this case, a significant part of the dye passed downwards, in the direction of the axial section.

### 3.6. Antibacterial Activity of Samples

To establish the bactericidal properties of the samples, which included chitosan, a test for antibacterial activity was carried out with a number of pathogenic bacteria. The purpose of this experiment was to establish the possibility of using chitosan-based samples that do not contain excipients that increase bactericidal properties, such as silver nanoparticles, for cell cultivation. Table 5 presents the results of measurement of the thickness of the zone of inhibition, obtained using the ImageJ program.

The analysis of the results of the microbiological study shows that samples based on chitosan exhibit antimicrobial activity against the studied pathogenic bacteria. The maximum thickness of the zone of inhibition was in the Alg-Ch-US sample in relation to all pathogenic bacteria; however, in relation to *Bacillus cereus*, the maximum thickness of the zone of inhibition was observed in Alg-Ch.

The smallest inhibition zone thickness values were recorded for Ch and Alg-Ch samples in relation to *Escherichia coli*. The results obtained correspond to the data presented

in [41–43]. The tests for antibacterial activity show that samples based on chitosan show resistance to pathogenic bacteria, which makes it possible to create favorable conditions for culturing cells in these matrices.

**Table 5.** Inhibition zone thickness.

No.	Inhibition Zone Thickness, mm			
	<i>Escherichia coli</i>	<i>Pseudomonas</i>	<i>Staphylococcus</i>	<i>Bacillus</i>
Ch	0.6	1.2	0.9	0.8
Ch-US	1.2	1.0	1.0	0.8
Alg-Ch	0.7	1.0	0.8	2.0
Alg-Ch-US	1.3	1.3	1.2	1.5

### 3.7. Results of the Study of Matrix Degradation in the DMEM Medium

A necessary step before culturing cells in matrices is to study the stability of these materials in the culture medium for at least three days, as well as to determine the change in the pH of the medium. The described preliminary study of materials allows one to select suitable matrix compositions, namely the types of polymers used, their mass ratio in the formed material and suitable cross-linking agents, before conducting studies on cells. This approach can significantly reduce the material and time costs for experiments on cell cultivation.

In the course of this work, the values of the change in the mass of samples and the pH of the culture medium DMEM were determined for three days (Figure 10).

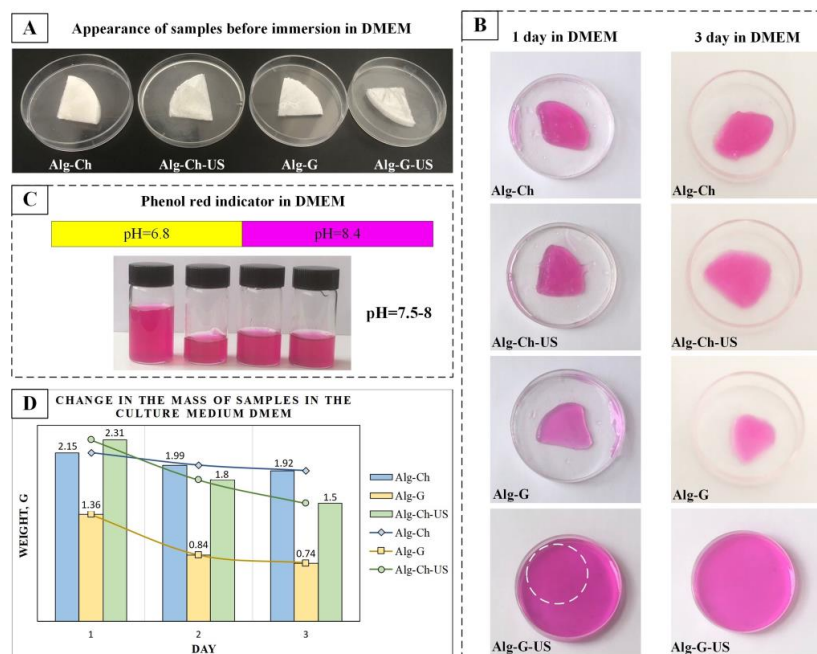


**Figure 10.** Investigation of sample degradation in DMEM culture medium: appearance of samples before immersion in DMEM (A), appearance and stability of samples in DMEM medium for three days (B), study of the effect of samples on the pH of the medium (C), diagram of sample mass change in within three days (D).

The results of the experiment in the culture medium show that the studied samples of Alg-Ch, Alg-Ch-US and Alg-G were stable for three days and retained their shape (Figure 10B) in relation to the original samples (Figure 10A). The Alg-G-US sample showed a loss of shape relative to the original sample, with the formation of a dense insoluble gel in the culture medium, which can be associated with the presence of wide cross-sectional channels in Alg-G-US.

The DMEM culture medium includes phenol red as a pH indicator. Therefore, the color of the medium, changing from bright yellow (pH = 6.8) to fuchsia (pH = 8.5), allows one to quickly determine the pH. The pH value of the medium was 7.5–8 and remained constant throughout the analysis (Figure 10C). Additionally, litmus test strips were used to measure the pH of the medium.

Based on the results of the experiment, a diagram was constructed showing the change in the mass of samples every 24 h in the culture medium for three days (Figure 10D). An analysis of the data obtained made it possible to determine that for the Alg-Ch-US and Alg-G samples, the decrease in mass was more intense. The values of changes in the weights of the Alg-Ch, Alg-Ch-US and Alg-G samples on the second day were 0.16, 0.51 and 0.52 g, respectively, and on the third day, 0.07, 0.3 and 0.1 g, respectively. However, the results also show that matrices based on Alg-Ch-US, Alg-G and Alg-G-US can be used in cell culture when it is necessary to replace the polymer scaffold with the resulting tissue. At the same time, the Alg-Ch sample is more suitable for cell cultivation without scaffold replacement.

### 3.8. Results of Cell Cultivation in Matrices

The results of cell cultivation in matrices based on alginate–gelatin and alginate–chitosan, as well as the results for the reference sample, plastic, are shown in Figure 11. The results of the study of the cultivation of fibroblast cells show that the samples do not show cytotoxic properties. However, all matrix samples, in comparison with the control sample (plastic), exhibit low adhesive properties. The samples based on alginate–gelatin promoted the adhesion of fibroblasts to a greater extent compared with samples based on alginate–chitosan. A higher degree of adhesion of matrices based on alginate–gelatin is associated with the existing sequence of RGD peptides (cell recognition sites). In the images shown (Figure 11), it can be seen that the fibroblasts located in the Alg-G and Alg-G-US matrices have an elongated fusiform shape, which means that the cells are in an activated state. The Alg-Ch and Alg-Ch-US samples also contain single cells that formed small clusters, but their shape is compressed spherical, indicating a possible stress on cells in these scaffolds.

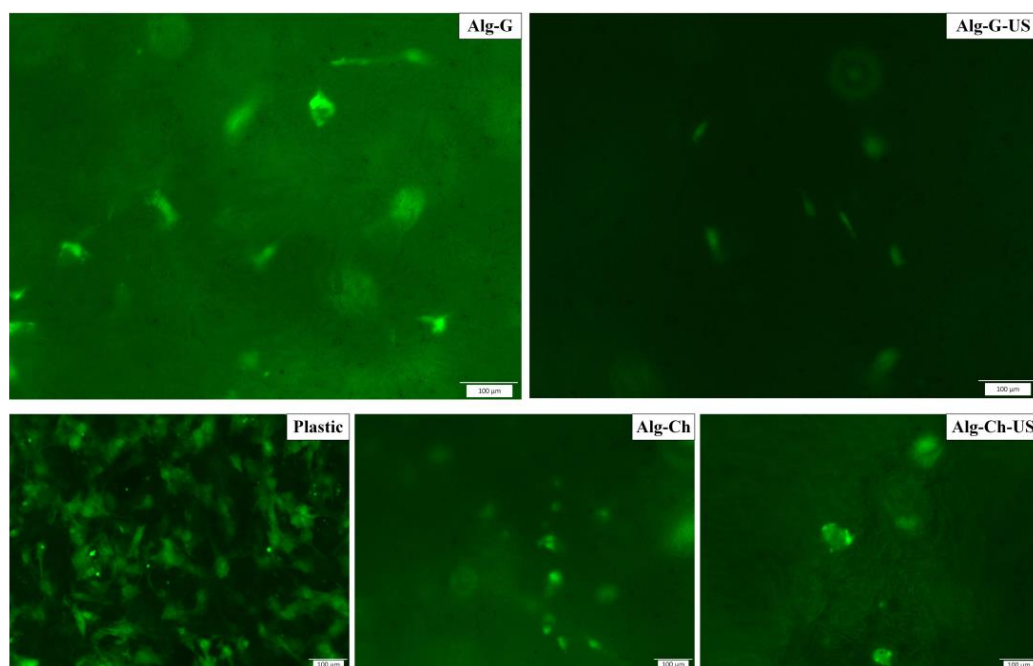


**Figure 11.** Results of culturing fibroblast cells in matrices (images of single fibroblast cells—magnification 100 µm).

#### 4. Conclusions and Prospects

The use of ultrasound at the stage of freezing the initial solutions of polysaccharides, before solvent sublimation, affected the microstructure of the formed ice crystals and, accordingly, the formed porous structure of the final materials. Ultrasound made it possible to achieve a uniform distribution of ice crystals in the volume of the sample and reduce their average size. SEM images confirmed the structuring of the plates of polymer components in both matrices. Studies of the porosity and sorption capacity of materials showed that ultrasound made it possible to increase the pore volume for a number of samples and, consequently, increased the value of the sorption capacity. When studying the permeability of the porous structure, the presence of wide transverse channels, which are mainly characteristic of a matrix based on alginate–gelatin, was found. The study of the stability of the samples in the culture medium made it possible to link the presence of wide channels in the alginate–gelatin sample with the loss of its shape. However, these results can be useful in the case when it is necessary to replace the polymer scaffold with the resulting tissue. The results of cell culture show that fibroblasts show a high degree of adhesion to alginate–gelatin-based matrices, but the overall degree of cell adhesion to matrices is assessed as low. In order to increase the degree of cell adhesion in further studies, edible gelatin will be replaced with another type of gelatin.

The study of the effect of ultrasound on the properties and structure of polysaccharides and materials based on them is an important task, the solution of which will make it possible to obtain a wide range of new hybrid and composite materials with different properties. Therefore, further studies of the dependence of the structure and properties of polysaccharides, which are of interest for tissue engineering and regenerative medicine, are needed.

**Author Contributions:** Conceptualization, M.G. and E.M.; methodology, M.G., E.M. and A.E.; formal analysis, N.M. and I.A.; investigation, E.M., M.G. and N.M.; writing, original draft—review and editing, E.M., M.G. and S.K. All authors have read and agreed to the published version of the manuscript.

**Funding:** Work on the cultivation of fibroblast cells was carried out under the grant of the Russian Science Foundation No. 22-15-00250.

**Institutional Review Board Statement:** Not applicable.

**Data Availability Statement:** The authors confirm that the data supporting the findings of this study are available within the article.

**Conflicts of Interest:** The authors declare no conflict of interest.

#### References

1. Bedian, L.; Villalba-Rodríguez, A.M.; Hernández-Vargas, G.; Parra-Saldivar, R.; Iqbal, H.M.N. Bio-Based Materials with Novel Characteristics for Tissue Engineering Applications—A Review. *Int. J. Biol. Macromol.* **2017**, *98*, 837–846. [[CrossRef](#)] [[PubMed](#)]
2. Silva, A.C.Q.; Silvestre, A.J.D.; Vilela, C.; Freire, C.S.R. Natural Polymers-Based Materials: A Contribution to a Greener Future. *Molecules* **2021**, *27*, 94. [[CrossRef](#)] [[PubMed](#)]
3. Farshidfar, N.; Iravani, S.; Varma, R.S. Alginate-Based Biomaterials in Tissue Engineering and Regenerative Medicine. *Mar. Drugs* **2023**, *21*, 189. [[CrossRef](#)] [[PubMed](#)]
4. Zielinski, B.A.; Aebischer, P. Chitosan as a Matrix for Mammalian Cell Encapsulation. *Biomaterials* **1994**, *15*, 1049–1056. [[CrossRef](#)]
5. Enrione, J.I.; Sáez, C.; López, D.; Skurtys, O.; Acevedo, C.; Osorio, F.; MacNaughtan, W.; Hill, S. Structural Relaxation of Salmon Gelatin Films in the Glassy State. *Food Bioprocess Technol.* **2012**, *5*, 2446–2453. [[CrossRef](#)]
6. Yamada, S.; Yamamoto, K.; Ikeda, T.; Yanagiguchi, K.; Hayashi, Y. Potency of Fish Collagen as a Scaffold for Regenerative Medicine. *BioMed Res. Int.* **2014**, *2014*, 302932. [[CrossRef](#)]
7. Andersen, T.; Auk-Emblem, P.; Dornish, M. 3D Cell Culture in Alginate Hydrogels. *Microarrays* **2015**, *4*, 133–161. [[CrossRef](#)]
8. Samimi, H.; Sohi, A.N.; Irani, S.; Arefian, E.; Mahdiannasser, M.; Fallah, P.; Haghpanah, V. Alginate-Based 3D Cell Culture Technique to Evaluate the Half-Maximal Inhibitory Concentration: An in Vitro Model of Anticancer Drug Study for Anaplastic Thyroid Carcinoma. *Thyroid Res.* **2021**, *14*, 27. [[CrossRef](#)]
9. Izzo, D.; Palazzo, B.; Scalera, F.; Gullotta, F.; Lapesa, V.; Scialla, S.; Sannino, A.; Gervaso, F. Chitosan Scaffolds for Cartilage Regeneration: Influence of Different Ionic Crosslinkers on Biomaterial Properties. *Int. J. Polym. Mater. Polym. Biomater.* **2019**, *68*, 936–945. [[CrossRef](#)]

10. Venkatesan, J.; Jayakumar, R.; Anil, S.; Chalisserry, E.P.; Pallela, R.; Kim, S.-K. Development of Alginate-Chitosan-Collagen Based Hydrogels for Tissue Engineering. *J. Biomater. Tissue Eng.* **2015**, *5*, 458–464. [[CrossRef](#)]
11. Nagai, N.; Nakayama, Y.; Zhou, Y.-M.; Takamizawa, K.; Mori, K.; Munekata, M. Development of Salmon Collagen Vascular Graft: Mechanical and Biological Properties and Preliminary Implantation Study. *J. Biomed. Mater. Res. B Appl. Biomater.* **2008**, *87B*, 432–439. [[CrossRef](#)]
12. Jiao, W.; Li, X.; Shan, J.; Wang, X. Study of Several Alginate-Based Hydrogels for In Vitro 3D Cell Cultures. *Gels* **2022**, *8*, 147. [[CrossRef](#)]
13. Xuan Du, D.; Xuan Vuong, B. Study on Preparation of Water-Soluble Chitosan with Varying Molecular Weights and Its Antioxidant Activity. *Adv. Mater. Sci. Eng.* **2019**, *2019*, 8781013. [[CrossRef](#)]
14. Gordienko, M.G.; Palchikova, V.V.; Kalenov, S.V.; Lebedev, E.A.; Belov, A.A.; Menshutina, N.V. The Alginate-Chitosan Composite Sponges with Biogenic Ag Nanoparticles Produced by Combining of Cryostructuration, Iontropic Gelation and Ion Replacement Methods. *Int. J. Polym. Mater. Polym. Biomater.* **2022**, *71*, 34–44. [[CrossRef](#)]
15. Wang, G.; Wang, X.; Huang, L. Feasibility of Chitosan-Alginate (Chi-Alg) Hydrogel Used as Scaffold for Neural Tissue Engineering: A Pilot Study in Vitro. *Biotechnol. Biotechnol. Equip.* **2017**, *31*, 766–773. [[CrossRef](#)]
16. Acevedo, C.A.; Díaz-Calderón, P.; López, D.; Enrione, J. Assessment of Gelatin-Chitosan Interactions in Films by a Chemometrics Approach. *CyTA J. Food* **2015**, *13*, 227–234. [[CrossRef](#)]
17. Li, L.; Chen, L.; Chen, X.; Chen, Y.; Ding, S.; Fan, X.; Liu, Y.; Xu, X.; Zhou, G.; Zhu, B.; et al. Chitosan-sodium Alginate-Collagen/Gelatin Three-Dimensional Edible Scaffolds for Building a Structured Model for Cell Cultured Meat. *Int. J. Biol. Macromol.* **2022**, *209*, 668–679. [[CrossRef](#)]
18. Samalens, F.; Thomas, M.; Claverie, M.; Castejon, N.; Zhang, Y.; Pigot, T.; Blanc, S.; Fernandes, S.C.M. Progresses and Future Prospects in Biodegradation of Marine Biopolymers and Emerging Biopolymer-Based Materials for Sustainable Marine Ecosystems†. *Green Chem.* **2022**, *24*, 1762–1779. [[CrossRef](#)]
19. Osman, M.A.; Virgilio, N.; Rouabhia, M.; Mighri, F. Development and Characterization of Functional Polylactic Acid/Chitosan Porous Scaffolds for Bone Tissue Engineering. *Polymers* **2022**, *14*, 5079. [[CrossRef](#)]
20. Candry, P.; Godfrey, B.J.; Wang, Z.; Sabba, F.; Dieppa, E.; Fudge, J.; Balogun, O.; Wells, G.; Winkler, M.K.H. Tailoring polyvinyl alcohol-sodium alginate (PVA-SA) hydrogel beads by controlling crosslinking pH and time. *Sci. Rep.* **2022**, *12*, 20822. [[CrossRef](#)]
21. Bahadoran, M.; Shamloo, A.; Nokoorani, Y.D. Development of a Polyvinyl Alcohol/Sodium Alginate Hydrogel-Based Scaffold Incorporating BFGF-Encapsulated Microspheres for Accelerated Wound Healing. *Sci. Rep.* **2020**, *10*, 7342. [[CrossRef](#)] [[PubMed](#)]
22. Alavarse, A.C.; Frachini, E.C.G.; da Silva, R.L.C.G.; Lima, V.H.; Shavandi, A.; Petri, D.F.S. Crosslinkers for Polysaccharides and Proteins: Synthesis Conditions, Mechanisms, and Crosslinking Efficiency, a Review. *Int. J. Biol. Macromol.* **2022**, *202*, 558–596. [[CrossRef](#)] [[PubMed](#)]
23. Venegas-Sánchez, J.A.; Tagaya, M.; Kobayashi, T. Ultrasound Stimulus Inducing Change in Hydrogen Bonded Crosslinking of Aqueous Polyvinyl Alcohols. *Ultrason. Sonochem.* **2014**, *21*, 295–309. [[CrossRef](#)] [[PubMed](#)]
24. Rokita, B.; Czechowska-Biskup, R.; Ulanski, P.; Rosiak, J.M. Modification of Polymers by Ultrasound Treatment in Aqueous Solution. *e-Polymers* **2005**, *5*, 261. [[CrossRef](#)]
25. Pita-López, M.L.; Fletes-Vargas, G.; Espinosa-Andrews, H.; Rodríguez-Rodríguez, R. Physically Cross-Linked Chitosan-Based Hydrogels for Tissue Engineering Applications: A State-of-the-Art Review. *Eur. Polym. J.* **2021**, *145*, 110176. [[CrossRef](#)]
26. Zhu, J.; Xiong, R.; Zhao, F.; Peng, T.; Hu, J.; Xie, L.; Xie, H.; Wang, K.; Jiang, C. Lightweight, High-Strength, and Anisotropic Structure Composite Aerogel Based on Hydroxyapatite Nanocrystal and Chitosan with Thermal Insulation and Flame Retardant Properties. *ACS Sustain. Chem. Eng.* **2020**, *8*, 71–83. [[CrossRef](#)]
27. Cai, B.; Mazahreh, J.; Ma, Q.; Wang, F.; Hu, X. Ultrasound-Assisted Fabrication of Biopolymer Materials: A Review. *Int. J. Biol. Macromol.* **2022**, *209*, 1613–1628. [[CrossRef](#)]
28. Zhang, L.; Qiao, Y.; Wang, C.; Liao, L.; Shi, D.; An, K.; Hu, J.; Wang, J.; Shi, L. Influence of High Hydrostatic Pressure Pretreatment on Properties of Vacuum-Freeze Dried Strawberry Slices. *Food Chem.* **2020**, *331*, 127203. [[CrossRef](#)]
29. Mou, X.; Chen, Z. Study on the Ultrasound-Assisted Drying Process of Deformable Porous Materials. *J. Food Eng.* **2021**, *306*, 110612. [[CrossRef](#)]
30. Geidobler, R.; Winter, G. Controlled Ice Nucleation in the Field of Freeze-Drying: Fundamentals and Technology Review. *Eur. J. Pharm. Biopharm.* **2013**, *85*, 214–222. [[CrossRef](#)]
31. Garcia-Noguera, J.; Oliveira, F.I.P.; Gallão, M.I.; Weller, C.L.; Rodrigues, S.; Fernandes, F.A.N. Ultrasound-Assisted Osmotic Dehydration of Strawberries: Effect of Pretreatment Time and Ultrasonic Frequency. *Dry. Technol.* **2010**, *28*, 294–303. [[CrossRef](#)]
32. Mokhova, E.; Gordienko, M.; Menshutina, N.; Gurskiy, I.; Tvorogova, A. Ultrasonic Freezing of Polymers of Various Compositions before Freeze Drying: Effect of Ultrasound on Freezing Kinetics and Ice Crystal Size. *Dry. Technol.* **2023**, 1–23. [[CrossRef](#)]
33. Legay, M.; Gondrexon, N.; Le Person, S.; Boldo, P.; Bontemps, A. Enhancement of Heat Transfer by Ultrasound: Review and Recent Advances. *Int. J. Chem. Eng.* **2011**, *2011*, 670108. [[CrossRef](#)]
34. Ruoslahti, E. The RGD Story: A Personal Account. *Matrix Biol.* **2003**, *22*, 459–465. [[CrossRef](#)]
35. Daemi, H.; Barikani, M. Synthesis and Characterization of Calcium Alginate Nanoparticles, Sodium Homopolymannuronate Salt and Its Calcium Nanoparticles. *Sci. Iran.* **2012**, *19*, 2023–2028. [[CrossRef](#)]
36. Ramli, R.H.; Phong Soon, C.; Mohd Rus, A.Z. Synthesis of Chitosan /Alginate/ Silver Nanoparticles Hydrogel Scaffold. *MATEC Web Conf.* **2016**, *78*, 01031. [[CrossRef](#)]

37. Yuvarani, I.; Kumar, S.S.; Venkatesan, J.; Kim, S.-K.; Sudha, P.N. Preparation and Characterization of Curcumin Coated Chitosan-Alginate Blend for Wound Dressing Application. *J. Biomater. Tissue Eng.* **2012**, *2*, 54–60. [[CrossRef](#)]
38. Wang, L.; Zhang, H.J.; Liu, X.; Liu, Y.; Zhu, X.; Liu, X.; You, X. A Physically Cross-Linked Sodium Alginate–Gelatin Hydrogel with High Mechanical Strength. *ACS Appl. Polym. Mater.* **2021**, *3*, 3197–3205. [[CrossRef](#)]
39. Chen, Q.; Tian, X.; Fan, J.; Tong, H.; Ao, Q.; Wang, X. An Interpenetrating Alginate/Gelatin Network for Three-Dimensional (3D) Cell Cultures and Organ Bioprinting. *Molecules* **2020**, *25*, 756. [[CrossRef](#)]
40. Beltran-Vargas, N.E.; Peña-Mercado, E.; Sánchez-Gómez, C.; Garcia-Lorenzana, M.; Ruiz, J.-C.; Arroyo-Maya, I.; Huerta-Yepey, S.; Campos-Terán, J. Sodium Alginate/Chitosan Scaffolds for Cardiac Tissue Engineering: The Influence of Its Three-Dimensional Material Preparation and the Use of Gold Nanoparticles. *Polymers* **2022**, *14*, 3233. [[CrossRef](#)]
41. Al-Gethami, W.; Al-Qasbi, N. Antimicrobial Activity of Ca-Alginate/Chitosan Nanocomposite Loaded with Camptothecin. *Polymers* **2021**, *13*, 3559. [[CrossRef](#)] [[PubMed](#)]
42. Zaghoul, E.H.; Ibrahim, H.H.A. Comparative Study on Antimicrobial Activity of Commercial and Extracted Chitin and Chitosan from *Marsupenaeus Japonicus* Shells. *Egypt. J. Aquat. Biol. Fish.* **2019**, *23*, 291–302. [[CrossRef](#)]
43. Zhang, M.-X.; Zhao, W.-Y.; Fang, Q.-Q.; Wang, X.-F.; Chen, C.-Y.; Shi, B.-H.; Zheng, B.; Wang, S.-J.; Tan, W.-Q.; Wu, L.-H. Effects of Chitosan-Collagen Dressing on Wound Healing in Vitro and in Vivo Assays. *J. Appl. Biomater. Funct. Mater.* **2021**, *19*, 228080002198969. [[CrossRef](#)] [[PubMed](#)]

**Disclaimer/Publisher’s Note:** The statements, opinions and data contained in all publications are solely those of the individual author(s) and contributor(s) and not of MDPI and/or the editor(s). MDPI and/or the editor(s) disclaim responsibility for any injury to people or property resulting from any ideas, methods, instructions or products referred to in the content.